

Electronic Supplementary Information†

Oxygen Electrocatalysis on (001)-Oriented Manganese Perovskite Films: Mn Valency and Charge Transfer at the Nanoscale

Kelsey A. Stoerzinger^{a,b}, Marcel Risch^b, Jin Suntivich^c, W. M. Lü^{d,e}, Jigang Zhou^f, Michael D. Biegalski^g, Hans M. Christen^g, Ariando^{h,e}, T. Venkatesan^{d,e,g}, Yang Shao-Horn^{a,b,i,1}

^a*Department of Materials Science & Engineering, Massachusetts Institute of Technology, 77 Massachusetts Ave., Cambridge, MA, 02139, USA*

^b*Electrochemical Energy Laboratory, Massachusetts Institute of Technology, 77 Massachusetts Ave., Cambridge, MA, 02139, USA*

^c*Harvard University Center for the Environment, 29 Oxford Street, Cambridge, MA, 02138, USA*

^d*Department of Electrical and Computer Engineering, National University of Singapore, 4 Engineering Drive 3, Singapore 117583, Singapore*

^e*NUSNNI-NanoCore, National University of Singapore, 5A Engineering Drive 1, Singapore 117411, Singapore*

^f*Canadian Light Source, 44 Innovation Boulevard, Saskatoon, SK, S7N 2V3, Canada*

^g*Center for Nanophase Materials Sciences, Oak Ridge National Laboratory, 1 Bethel Valley Road, Oak Ridge, TN, 37831, USA*

^h*Department of Physics, National University of Singapore, 2 Science Drive 3, Singapore 117542, Singapore*

ⁱ*Department of Mechanical Engineering, Massachusetts Institute of Technology, 77 Massachusetts Ave., Cambridge, MA, 02139, USA*

¹To whom correspondence may be addressed. Email: shaohorn@mit.edu

Estimation of Effective Junction Resistance

The thermionic emission equation is applied to estimate the effective resistance of the junction between NSTO and the $[\text{Fe}(\text{CN})_6]^{3-/4-}$ redox:

$$I = R^*T^2 \exp\left(\frac{-e|\phi_{\text{NSTO}} - \phi_{\text{Fe}(\text{CN})_6}|}{kT}\right) \left(\exp\left(\frac{(V - E_{\text{Fe}(\text{CN})_6}^0)}{kT}\right) - 1\right) \quad \text{Eq. (S1)}$$

where R^* is the Richardson constant ($\approx 120 m^*/m_0 Acm^{-2}K^{-2}$), ϕ represents the Fermi level, V is the applied potential, and $E_{\text{Fe}(\text{CN})_6}^0$ is the redox potential for $[\text{Fe}(\text{CN})_6]^{3-/4-}$ (~ 1.2 V vs. RHE). As the effective mass of electron in NSTO is estimated to be ~ 7.5 ,¹ the calculated effective resistance from the thermionic emission is estimated to be ~ 1 k Ω cm⁻². We note, however, that the electro-kinetics also depends on the kinetics of the $[\text{Fe}(\text{CN})_6]^{3-/4-}$ redox as well as the field emission contribution to the Schottky barrier; separating these contributions will require a much more rigorous mathematical treatment that is beyond the scope of this work.

Influence of LMO Film on the Electrode/Electrolyte Barrier

In the NSTO/LMO/ $\text{Fe}(\text{CN})_6$ configuration, the incipient p-type LMO would donate electrons to the electrolyte, and form a depletion layer near the surface, while the NSTO substrate could also donate its electrons to LMO. This forms two junctions in series with one another, each with $\Delta\phi_1 = \phi_{\text{NSTO}} - \phi_{\text{LMO}}$ and $\Delta\phi_2 = \phi_{\text{LMO}} - \phi_{\text{Fe}(\text{CN})_6}$ barriers. This is in contrast to NSTO/ $\text{Fe}(\text{CN})_6$, which only has one junction $\Delta\phi = \phi_{\text{NSTO}} - \phi_{\text{Fe}(\text{CN})_6}$. The positive contribution from a two-junction configuration to electron transfer is examined using a series of two rectifying junctions. We begin with the description for an individual junction:

$$I = I_0 \left(\exp\left(\frac{V}{kT}\right) - 1\right) = I'_0 \exp\left(-\frac{\Delta\phi}{kT}\right) \left(\exp\left(\frac{V}{kT}\right) - 1\right) \quad \text{Eq. (S2)}$$

$$R = \frac{dV}{dI} = \frac{kT}{I'_0} \exp\left(\frac{\Delta\phi}{kT}\right) \exp\left(-\frac{V}{kT}\right) \quad \text{Eq. (S3)}$$

where I'_0 is the reverse bias saturation current, V is the applied potential, and R is the effective resistance. We can then estimate the effective resistance of the two junctions in series:

$$R' = \frac{kT}{I'_1} \exp\left(\frac{\Delta\phi_1}{kT}\right) \exp\left(-\frac{V_1}{kT}\right) + \frac{kT}{I'_2} \exp\left(\frac{\Delta\phi_2}{kT}\right) \exp\left(-\frac{V_2}{kT}\right) \quad \text{Eq. (S4)}$$

Taking the ratio between two junctions (describing NSTO/LMO/ $\text{Fe}(\text{CN})_6$) to a single junction (describing NSTO/ $\text{Fe}(\text{CN})_6$), we find:

$$\frac{R'}{R} = \frac{I'_0}{I'_1} \exp\left(\frac{\Delta\phi_1 - \Delta\phi}{kT}\right) \exp\left(-\frac{V_1 - V}{kT}\right) + \frac{I'_0}{I'_2} \exp\left(\frac{\Delta\phi_2 - \Delta\phi}{kT}\right) \exp\left(-\frac{V_2 - V}{kT}\right) \quad \text{Eq. (S5)}$$

Using $V = V_2 + V_1$ and $\Delta\phi = \Delta\phi_1 + \Delta\phi_2$:

$$\frac{R'}{R} = \frac{I'_0}{I'_1} \exp\left(\frac{V_2 - \Delta\phi_2}{kT}\right) + \frac{I'_0}{I'_2} \exp\left(\frac{V_1 - \Delta\phi_1}{kT}\right) \quad \text{Eq. (S6)}$$

We assume that the ratio I'_0/I'_1 is close to unity. Within the limit of $V < \Delta\phi_1$ and $\Delta\phi_2$, we arrive at an approximation that R'/R is smaller than 1, and thereby,

$$R_{\text{NSTO-LMO-Fe}(\text{CN})_6} = R_{\text{NSTO-LMO}} + R_{\text{LMO-Fe}(\text{CN})_6} < R_{\text{NSTO-Fe}(\text{CN})_6}$$

Thus, the presence of the LMO reduces the barrier due to electron depletion seen by NSTO, allowing charge to transfer in and out of the electrode surface more effectively.

For the thinner LMO films, the continuity equation above approaches the limit in which space charge layers between NSTO/LMO and LMO/Fe(CN)₆ begin to overlap and eventually behave as if there is no LMO layer on NSTO. Hence, thinner films are expected to exhibit similar behavior to NSTO, which has a large band bending barrier and consequently, sluggish electron transfer kinetics. From the energy viewpoint, as the work function of NSTO (4.1 eV) is less than that of LMO (4.5 eV), electrons will be transferred from the high Nb 4d donor state into LMO. This would raise the E_F of LMO with decreasing thickness. Thus, the facile transfer of electrons between LMO and NSTO may increase at the expense of the charge transfer and resultant band bending between LMO and the electrolyte. As a result of this band shifting, $\phi_{LMO-Fe(CN)_6}$ approaches $\phi_{NSTO-Fe(CN)_6}$, and $\phi_{NSTO-LMO}$ becomes a vanishing quantity, and the electron becomes ridden with a barrier, similar to NSTO/Fe(CN)₆ junction, for electron transfer to the electrolyte. The thinner the LMO films, the larger the barrier becomes, which is prohibitive for electron transfer to the electrolyte. We use this simple reasoning to explain increasing electron transfer difficulty in the redox of [Fe(CN)₆]^{3-/4-} with thinner films. We caution however that our model is overly simplistic and is provided only as an appeal to the readers' intuition. Detailed electronic structure calculation would be essential to capture the rich physics at the interface between NSTO/LMO/Fe(CN)₆ to include issues such as the shifting E_F that is likely to be accompanied by an increased band gap, similar to that of MnO, ~3.9 eV.²

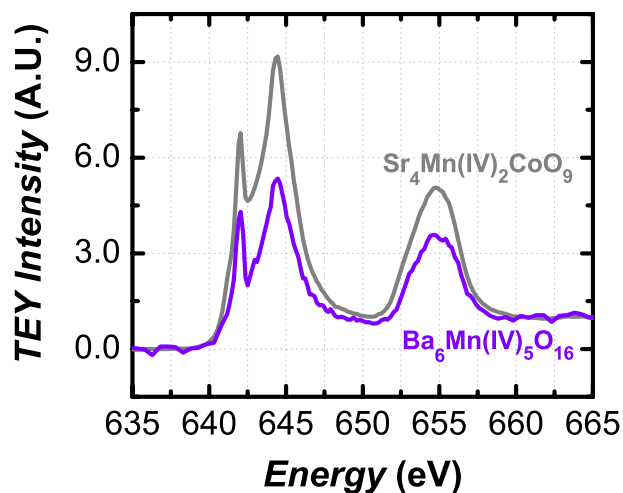


Fig. S1: X-ray absorption spectra (XAS) acquired in total electron yield (TEY) mode at Mn L-edges, showing the comparable Mn⁴⁺ spectra for Sr₄Mn(IV)₂CoO₉ (—), known to charge disproportionate into Mn⁴⁺ and Co²⁺,³ also shown in Fig. 6 of the main text, and Ba₆Mn(IV)₅O₁₆ (—).

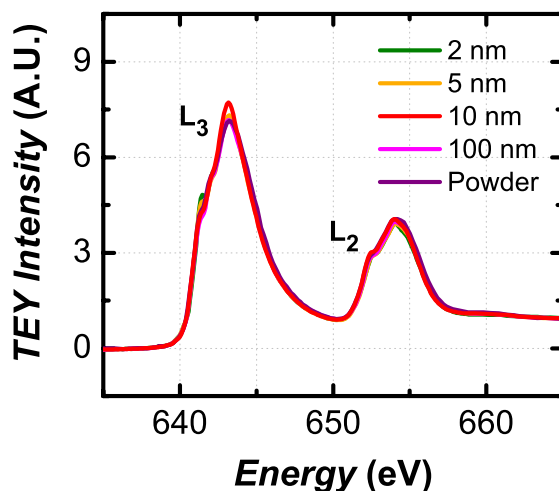


Fig. S2: X-ray absorption spectra (XAS) acquired in total electron yield (TEY) mode at Mn L-edges, showing the comparable Mn^{3+} spectra for a 100 nm LMO film (—) and LMO powder (—), used to align the energy scale at the ALS to that of the CLS in order to compare with a Mn^{4+} reference. LMO films of 2 (—), 5 (—), and 10 nm (—) thickness, shown in Fig. 6 of the main text, show predominately Mn^{3+} character. The large intensity ratio of $I(L_3)/I(L_2)$ establishes clearly that Mn^{3+} is predominantly in the high spin state.^{4,5}

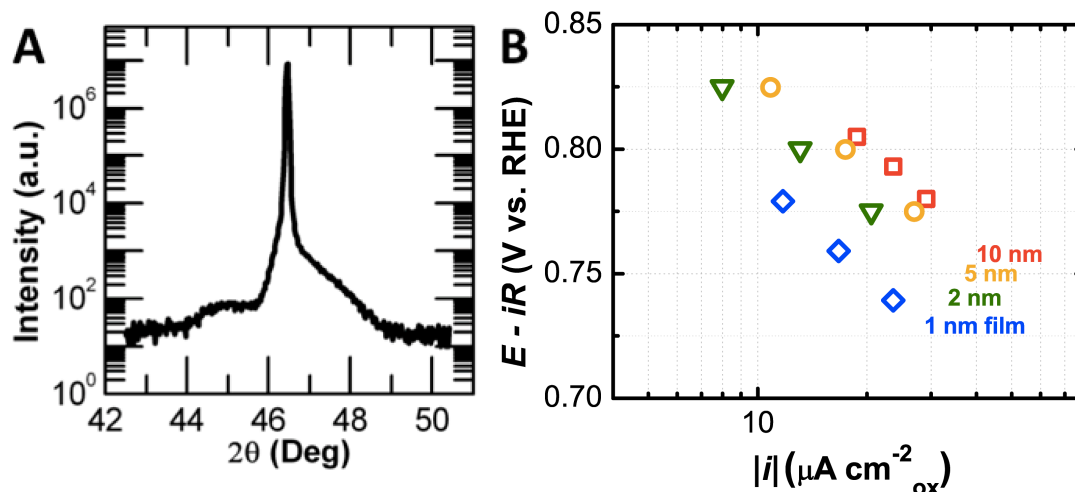


Fig. S3: Characterization of LaMnO_3 (LMO) films. (A) Thin film X-ray diffraction (XRD) in a coupled 2θ - ω configuration around the (002) Bragg peak of the Nb-doped SrTiO_3 (NSTO) substrate for a 5 nm LMO film. The near matching of lattice constants suggests negligible strain. Films show good epitaxy, and thickness fringes further confirm high quality. (B) ORR activity for a second set of LMO films deposited at Oak Ridge National Labs, including the 5 nm film from panel (A). A Tafel plot from chronoamperometry (constant applied voltage) shows the ohmic corrected applied voltage ($E-iR$) vs. current ($|i|$) on a logarithmic scale. The trend of decreasing activity with thickness is consistent with that of the films grown at the National University of Singapore, presented in Fig. 3 of the main text.

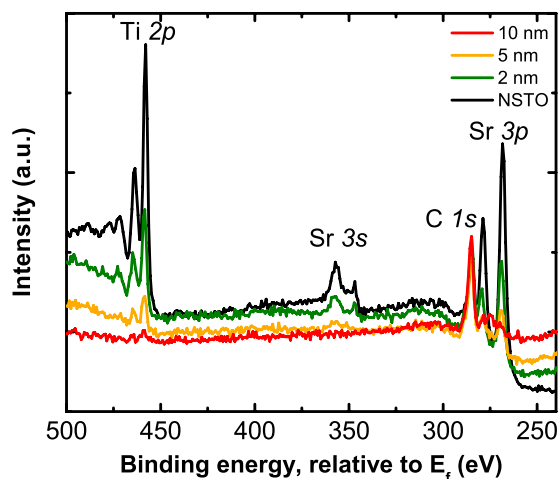


Fig. S4: X-ray photoemission spectroscopy (XPS) of LMO films of 2 (—), 5 (—), and 10 nm (—) thickness, as well as a blank NSTO substrate (—). Some signal from the substrate is observed for all films, which is not surprising considering the inelastic mean free path for a band gap ~ 1 eV (bulk LMO) ⁶ and an incident energy of 1.5 keV is nearly 3 nm. The consistent ratio of Sr:Ti in the films confirms no preferential segregation from the substrate during deposition.

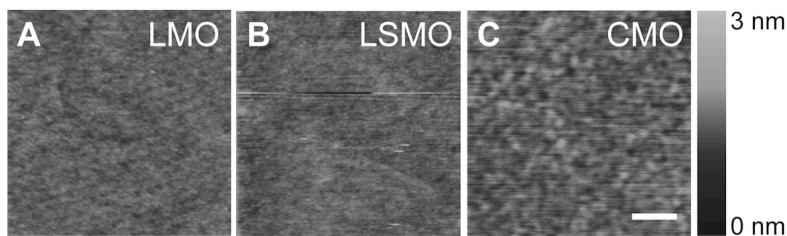


Fig. S5: Atomic force microscopy (AFM) images in tapping mode of 5 nm films of (A) LaMnO_3 (LMO), (B) $\text{La}_{0.67}\text{Sr}_{0.33}\text{MnO}_3$ (LSMO), and (C) CaMnO_3 (CMO). The scale bar is the same for all figures and is 200 nm in length. The brightness scale bar is 0–3 nm.

Table S1: Quantification of topography from AFM of LMO, LSMO, and CMO 5 nm films

Material	Maximum height (nm)	RMS roughness (nm)
LMO	1.55	0.13
LSMO	3.29	0.17
CMO	1.83	0.20
NSTO (bare)	1.17	0.16

Table S2: Quantification of topography from AFM of LMO films

Thickness (nm)	Maximum height (nm)	RMS roughness (nm)
1	1.47	0.16
2	1.45	0.15
5	1.55	0.13
10	1.90	0.15
NSTO (bare)	1.17	0.16

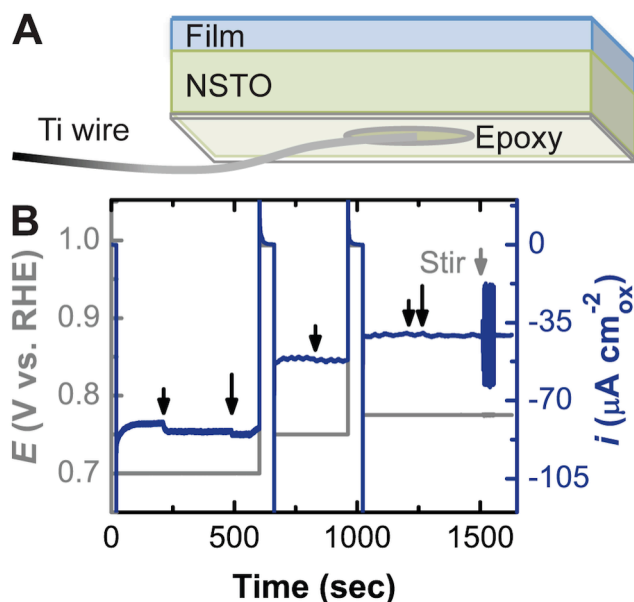


Fig. S6: Making electrical contact and measuring O_2 diffusion limitations. (A) Electrode schematic, showing the electrical contact to the back of the Nb-doped SrTiO_3 (NSTO) substrate, and epoxy covering all but the front face of the catalyst film. (B) Plot of the applied voltage (left axis, —) and current (right axis, —) vs. time, where the flow of O_2 or stir rate of the O_2 -saturated 0.1 M KOH electrolyte was increased at each time annotated by arrows. For absolute currents $\leq 0.04 \text{ mA cm}^{-2}_{\text{ox}}$, the current is independent of reactant flux and can be considered kinetically limited in this regime.

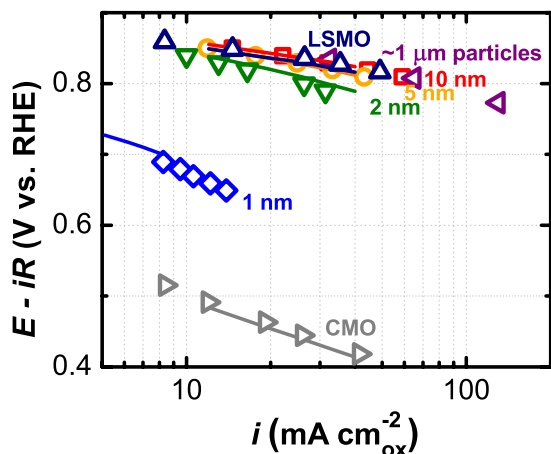


Fig. S7: Tafel plot comparing measurements from current-voltage (CV) scans at 10 mV/s (lines) to those from chronoamperometry (constant applied voltage, points), showing ohmic-corrected applied voltage vs. absolute current on a logarithmic scale. The two methods yield identical measurements of ORR activity. Films are 5 nm CMO (—), 5 nm LSMO (—), and LMO of 1 (—), 2 (—), 5 (—), and 10 nm (—) thickness.

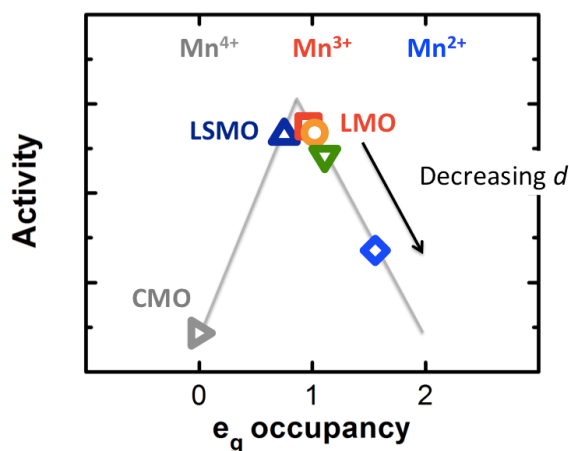


Fig. S8: Schematic of the volcano relationship for ORR activity of $d = 5$ nm CaMnO_3 (CMO), 5 nm $\text{La}_{0.67}\text{Sr}_{0.33}\text{MnO}_3$ (LSMO), and LaMnO_3 (LMO) films of 10 (red), 5 (orange), 2 (green) and 1 nm (blue) thickness. The activity can be described by e_g orbital occupancy, as found previously by Suntivich et al.,⁷ which is estimated from the Mn valence state (assuming high spin in all cases). The optimal e_g at the tip of the volcano is ~ 1 , for Mn^{3+} .

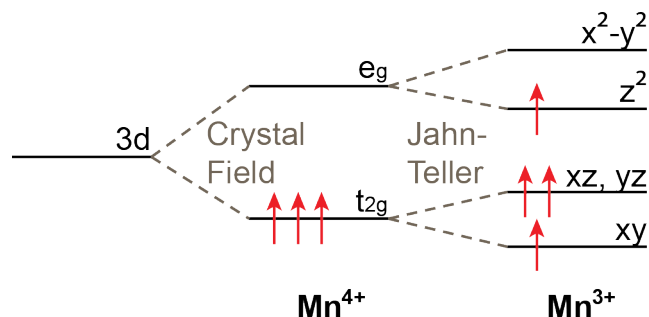


Fig. S9: Energy splitting of the 3d-electron states in an octahedral crystal field (Mn^{4+} , as in CaMn(IV)O_3) and due to the Jahn-Teller effect (Mn^{3+} , as in LaMn(III)O_3). For Mn^{3+} , both the occupied z^2 and unoccupied x^2-y^2 orbital are of e_g parentage.

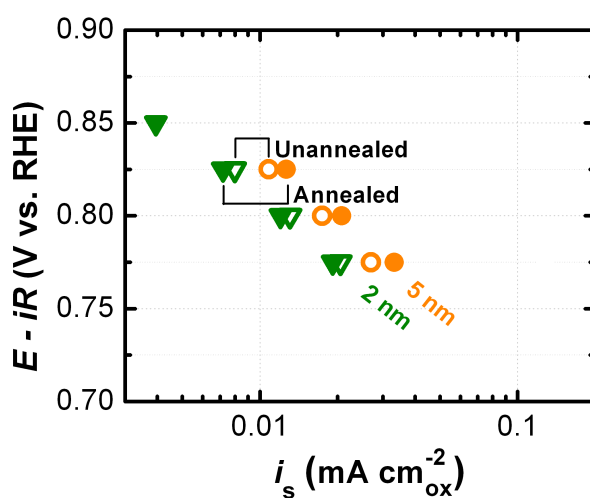


Fig. S10: ORR activity for LMO films deposited at Oak Ridge National Labs on as-received (open) and annealed, terraced NSTO substrates (solid). A Tafel plot from chronoamperometry (constant applied voltage) shows the ohmic corrected applied voltage ($E-iR$) vs. absolute current ($|i_s|$) on a logarithmic scale. The measured activity is comparable for the two topographies, and the same trend of decreasing activity with film thickness is observed, suggesting the origin is not geometric.

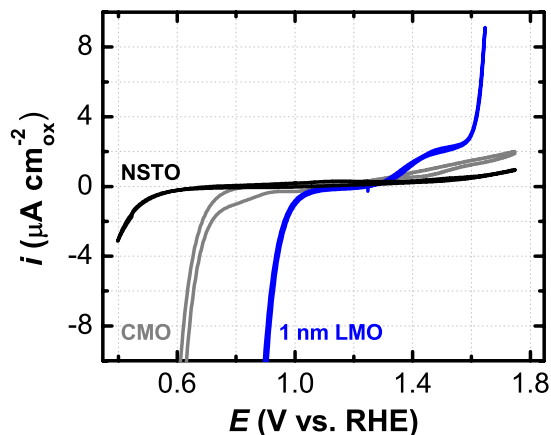


Fig. S11: Cycling voltammetry (CV) showing the onset of current for the $[\text{Fe}(\text{CN})_6]^{3-/4-}$ redox couple on a blank NSTO substrate (—), as well as a 5 nm CMO film (—) and 1 nm LMO film (—). Measurements were performed at 10 mV/s in Ar-saturated 0.1 M KOH with 5 mM each of $\text{K}_4[\text{Fe}(\text{CN})_6]$ and $\text{K}_3[\text{Fe}(\text{CN})_6]$. For a blank NSTO substrate, ~ 0.7 V beyond the equilibrium voltage must be applied to achieve reduction current. This is approximately equal to the magnitude of band bending that results from charge depletion at the electrolyte interface, where the difference in work function, ϕ , between the NSTO substrate and $[\text{Fe}(\text{CN})_6]^{3-/4-}$ is approximately 0.8 V, as shown in Fig. 5A of the main text.

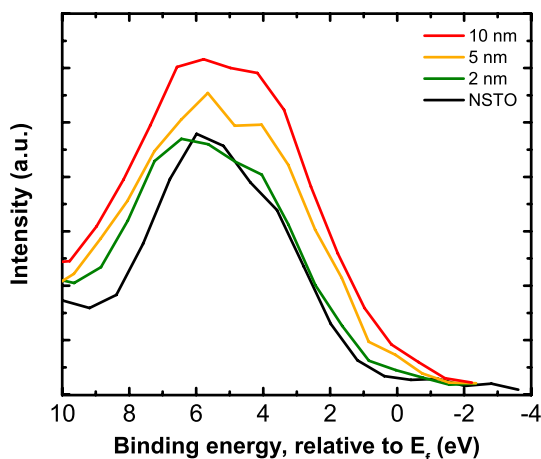


Fig. S12: XPS of LMO films of 2 (—), 5 (—), and 10 nm (—) thickness, as well as a blank NSTO substrate (—). The binding energy is calibrated to the Fermi level, E_F , by defining the binding energy of adventitious carbon to 285 eV.⁸ As film thickness decreases, the Valence band edge shifts farther from E_F . This suggests a transition in the semiconductor to more n-type behavior, consistent with electron donation from the NSTO substrate.

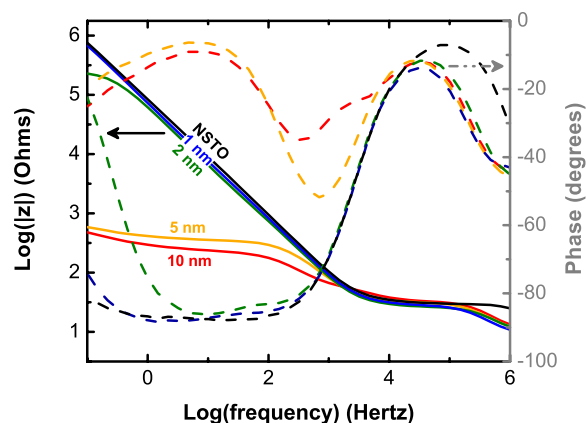


Fig. S13: Electrical impedance spectroscopy (EIS) presented as a Bode plot: solid lines (left axis) show the magnitude of impedance, $|z|$, on a log scale vs. frequency on a log scale, and dashed lines (right axis) plot the phase against the same abscissa. EIS was taken at the open circuit voltage (1.2 V vs. RHE) in 0.1 M KOH with the $[\text{Fe}(\text{CN})_6]^{3-/4-}$ redox couple for LMO films of 10 (—), 5 (—), 2 (—), and 1 nm (—) thickness, as well as a blank NSTO substrate (—). Similar to the NSTO substrate, the 1 and 2 nm films exhibit strong capacitive behavior. The impedance intercept projected from linear regime gives a capacitance of 1.7 μF for the NSTO, increasing to 3.5 μF for the 2 nm film.

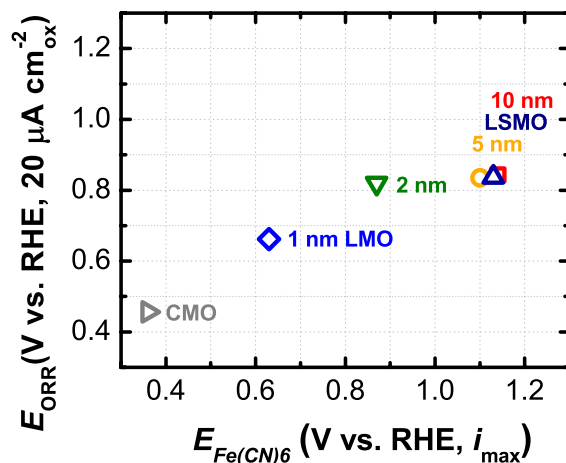


Fig. S14: Plot of the potential required to achieve $20 \mu\text{A}/\text{cm}^2_{\text{ox}}$ of oxygen reduction current from capacitance-corrected CVs, E_{ORR} , vs. the potential corresponding to the maximum reduction current of $[\text{Fe}(\text{CN})_6]^{3-}$, $E_{\text{Fe}(\text{CN})_6}$. For LMO films 1 and 2 nm in thickness, as well as CMO, depletion at the electrode/electrolyte interface leads to a large barrier in charge transfer, reflected in the reduction of $E_{\text{Fe}(\text{CN})_6}$. These films also show diminished ORR activity, represented by E_{ORR} . The ORR activity is also reduced when $\text{LaMn}(\text{III})\text{O}_3$ is doped with either electrons (thinner films, $\text{LaMn}(\text{II,III})\text{O}_3$) or holes ($\text{CaMn}(\text{IV})\text{O}_3$).

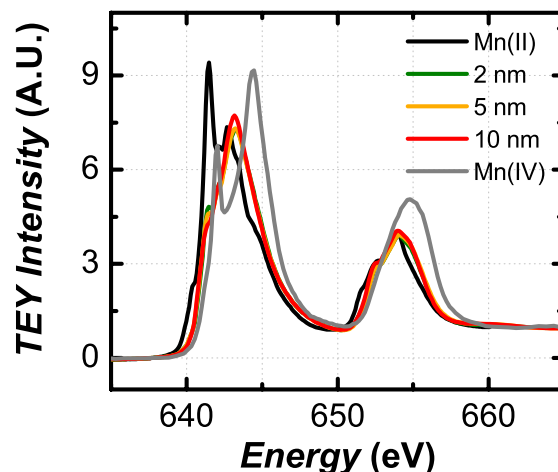


Fig. S15: X-ray absorption spectra (XAS) acquired in total electron yield (TEY) mode at Mn L-edges, showing an extended range compared to that in Figure 6 of the main text. LMO films of 2 (—), 5 (—), and 10 nm (—) thickness are compared to references of Mn(II)O (—) and Sr₄Mn(IV)₂CoO₉ (—). The increase in amplitude at ~641.5 eV indicates that thinner films are characterized by conversion of Mn³⁺ to Mn²⁺. Electrochemical measurements for this set of films are presented in Figure S1B.

References

1. S. Ohta, T. Nomura, H. Ohta and K. Koumoto, *Journal of Applied Physics*, 2005, **97**, 034106-034104.
2. J. van Elp, R. H. Potze, H. Eskes, R. Berger and G. A. Sawatzky, *Physical Review B*, 1991, **44**, 1530-1537.
3. K. Boulahya, M. Parras, J. M. González-Calbet and J. L. Martínez, *Chemistry of Materials*, 2003, **15**, 3537-3542.
4. B. T. Thole and G. van der Laan, *Physical Review B*, 1988, **38**, 3158-3171.
5. R. Qiao, T. Chin, S. J. Harris, S. Yan and W. Yang, *Current Applied Physics*, 2013, **13**, 544-548.
6. T. Kida, G. Guan and A. Yoshida, *Chemical Physics Letters*, 2003, **371**, 563-567.
7. J. Suntivich, H. A. Gasteiger, N. Yabuuchi, H. Nakanishi, J. B. Goodenough and Y. Shao-Horn, *Nat Chem*, 2011, **3**, 546-550.
8. G. Johansson, J. Hedman, A. Berndtsson, M. Klasson and R. Nilsson, *Journal of Electron Spectroscopy and Related Phenomena*, 1973, **2**, 295-317.